JOURNAL OF CATALYSIS 75, 382–395 (1982)

Further Studies of the Nickel/Graphite–Hydrogen Reaction

R. T. K. BAKER, R. D. SHERWOOD, AND E. G. DEROUANE[1]

Corporate Research-Science Laboratories, Exxon Research and Engineering Company, Linden, New Jersey 07036

Received August 27, 1981; revised February 15, 1982

A combination of electron microscopy and hydrogen chemisorption techniques has been used to probe the causes for the unusual loss in catalytic activity of nickel particles in the graphite–hydrogen reaction. This deactivation, which occurs at about 1000°C, is associated with the spreading of material along the sides of channels created catalytically at lower temperatures. Detailed quantitative analysis of this phenomenon indicates that nickel is progressively laid down as a near-monolayer film on the walls of the channels while the particles move forward. Nickel deposited in this manner strongly interacts with hydrogen "sorbed" by the graphite and therefore has a poor activity for C–C bond rupture (carbon gasification) and a low hydrogen chemisorption capacity. Removal of "sorbed" hydrogen at 1000°C, under vacuum or in inert gas environments, not only results in carbon gasification, but also in removal of Ni–H interactions and formation of Ni–C bonds (a surface carbide which does not adsorb H_2). These Ni–C bonds are broken by steaming at 1000°C and the hydrogen chemisorption capacity is restored.

INTRODUCTION

In earlier studies, the anomalous behavior of catalytically active nickel particles during the hydrogenation of graphite at high temperatures has been reported (*1*, *2*). Using controlled-atmosphere electron microscopy, it was possible to directly observe the gradual depletion in size of nickel particles which were in the act of propagating channels across the graphite basal plane. In subsequent experiments, this apparent particle loss was shown to be caused by wetting and spreading of nickel on the graphite resulting in the formation of a thin film of metal along the channel walls. Restoration of particles was achieved by replacing hydrogen with oxygen or steam and raising the temperature to 850°C (*2*).

In an attempt to learn more about this unusual nickel–carbon interaction, we have conducted a more comprehensive electron microscopic investigation than had previously been performed and combined this with a detailed quantitative analysis of the wetting and spreading phenomenons. We have also used hydrogen chemisorption techniques in an effort to identify the adsorption characteristics of nickel in the thin-film form.

EXPERIMENTAL

Electron Microscopy Studies

Detailed dimensions of channels created by active nickel particles were determined from shadowing experiments on specimens which had been reacted in hydrogen in the CAEM (*3*). This operation was accomplished by evaporating uranium atoms onto the specimen at an angle of 25 ± 2° with respect to the plane of the graphite surface. Areas of the specimen shielded from the impinging beam of atoms by surface relief or depression features were not coated, and, as a consequence appeared as enlarged shadows when the specimen was examined in the transmission electron microscope.

Transmission specimens of single-crystal graphite (Ticonderoga, N.Y.) were prepared by a standard method (*4*). Nickel was introduced onto these specimens by evapo-

[1] On leave from Facultes Universitaires de Namur, Department of Chemistry, Namur, Belgium.

0021-9517/82/060382-14$02.00/0

ration of spectrographically pure nickel from a tungsten filament at a residual pressure of 5×10^{-6} Torr in sufficient quantity to produce a monolayer film.

The reactant gas used in this portion of the work, hydrogen, was obtained from Scientific Gas Products with a stated purity of 99.99% and was used without further purification.

Hydrogen Chemisorption Experiments

Catalyst preparation. Grafoil (Union Carbide, New York, N.Y., GTA grade) was selected as the carbonaceous medium as single-crystal graphite was not in sufficient supply for bulk experiments. A nickel-on-Grafoil catalyst was prepared by adsorption from a 10% solution of nickel acetate in methanol on 5-mm disks of Grafoil, at 80°C. After drying at 120°C for 8 hr the catalyst was washed several times with methanol to remove the excess nickel salt. The nickel content, in the so-obtained unreduced material, was 2.67 wt%.

Reduction and chemisorption procedures. Fresh catalyst, 2.5 g, was reduced at 600°C for 2.0 hr under a pure hydrogen flow (30 liters · hr^{-1}). The reduced sample was then evacuated for 0.5 hr at 550°C and at room temperature for 0.25 hr before the first hydrogen chemisorption (C_1) was made. These measurements were made in a conventional glass vacuum system described previously (*5*). In order to evaluate the amount of strongly bound hydrogen, a second hydrogen chemisorption (C_2) was performed after evacuation of the sample at room temperature. A period of 30 min was allowed for the system to reach equilibrium before any adsorption measurement was made.

Next, the sample was treated at 1095°C for 2 hr under flowing hydrogen (30 liters · hr^{-1}), evacuated at 550°C for 0.5 hr, and at room temperature for 0.25 hr. Hydrogen chemisorption (C_3) was again performed, followed by evacuation at room temperature and another chemisorption (C_4) in order to evaluate the amount of strongly held hydrogen.

The sample was subsequently heated at 1000°C for 2.0 hr under flowing hydrogen (18 liters · hr^{-1}), evacuated at 550°C for 0.5 hr, and heated to 1000°C in a closed system while the pressure increase (due to H_2 desorption or CH_4 formation) was continuously monitored for about 2 hr (D_1). The sample was then evacuated at 1000°C (0.1 hr) and at room temperature (0.25 hr) before a further hydrogen chemisorption (C_5) was performed.

The sample was finally treated with steam (He, 30 liters · hr^{-1}, passed through a bubbler containing water at 25°C) at 800°C for 1.0 hr, flushed with helium at 300°C for 0.25 hr, and evacuated at room temperature for 0.2 hr, at which point a further hydrogen chemisorption was made (C_6). Subsequently, the same treatment was repeated, although the steaming temperature was raised to 1000°C, and a final hydrogen chemisorption (C_7) carried out.

This whole procedure was repeated for another sample (1.1 g); however, in this case the desorption step at 1000°C (D_1) was omitted. Hydrogen chemisorption isotherms were obtained after treatment in hydrogen at 1000°C (1 hr, 30 liters · hr^{-1}) (C_3'), evacuation at room temperature following steaming (C_6'), and further treatment of the steamed catalyst in H_2 at 600°C, or 2.0 hr (30 liters · hr^{-1}) (C_8'). All these treatments are summarized in Table 1. All evacuation steps were carried out at a pressure value lower than 5×10^{-6} Torr. In order to normalize the chemisorption data, the sample weight was recorded after each adsorption run. After completion of the chemisorption experiments specimens were examined by X-ray diffraction.

For these reduction and chemisorption studies, hydrogen of 99.95% purity was passed through a Deoxo unit (Engelhard Industries, Inc., Murray Hill, N.J.), a 5A molecular sieve drying trap, an Oxy-trap (Alltech Associates, Arlington Heights, Ill.) to remove the last traces of oxygen, and

TABLE 1

Treatments and Hydrogen Chemisorption Data on Nickel/Grafoil Specimens

Sample No.	Treatment before H_2 chemisorption[a]	Temperature (°C)	Measurement[b]
1	Reduction in H_2	600	C_1, C_2
	High-temperature treatment in H_2	1095	C_3, C_4
	High-temperature evacuation	1000	D_1, C_5
	Steaming (He/H_2O, 32:1)	800	C_6
	Steaming (He/H_2O, 32:1)	1000	C_7
2	High-temperature treatment in H_2	1095	C_3'
	Steaming (He/H_2O, 32:1)	1000	C_6'
	Reduction in H_2	600	C_8'

[a] Successive experiment/treatments in samples 1 and 2.
[b] C = H_2 chemisorption at 25°C; D = desorption of H_2 at indicated temperature.

finally through a liquid nitrogen trap (before being admitted to the catalyst for reductions or chemisorption measurements). Helium of 99.999% purity was used after passage through a 5A molecular sieve drying trap.

RESULTS AND DISCUSSION

Electron Microscopy Studies of Channel Geometry

Figure 1 is a micrograph of a shadowed specimen showing a channel produced after heating the nickel/graphite system to 1050°C in 1.0 Torr hydrogen. The arrows indicate the direction of the shadow across the surface and were determined from the shadows of several particles. In order to clarify the understanding of some of the salient features exhibited in this micrograph, the channel has been divided into regions, A to D, where A represents the initial stages and D the termination of the channel. The depth of the channel can be readily calculated from a knowledge of the angle of incidence and the width of the shadow, using a simple trigonometrical relationship. In this case the depth was found to be 35 ± 3 nm, and the ratio of channel depth to width is then about 0.25 to 0.3.

Other aspects which emerge from inspection of the micrograph are:

(i) The shadow in region D is linear indicating that the channel walls are vertical.

(ii) The unshaded region between A and B has a constant width; hence the channel depth is constant up to the stage where the particle starts to exhibit anomalous behavior (region C).

(iii) The channel collapses in region C and this period may correspond to the progressive relaxation of the catalyst particle as material is progressively laid down on the channel walls. Eventually when it reaches a critical size it proceeds to follow an uncontrolled course, region D.

Analysis of the Electron Microscopy Data

(A) Nickel particle–graphite interaction. A much clearer understanding of the intricate steps involved in the behavioral pattern of active nickel particles can be gained from analysis of the CAEM data, where the process was followed continuously. Earlier dynamic studies demonstrated the existence of a nickel–graphite wetting phenomenon which was directly responsible for the loss of catalytic activity of the metal toward graphite gasification (*1*, *2*). There is little doubt that the wetting effect is associated with a strong nickel–graphite interaction, which can be best understood from the following theoretical treatment.

Our data indicate that nickel particles which *wet* graphite have a contact angle, Θ, of 75 ± 5°, whereas those particles which *do not wet* the support exhibit a contact angle of 120 ± 10° and also appear to be inactive. The following values of Θ, are reported in the literature:

68° (1500°C) for Ni/graphite in H_2 (*6*),

90° (1500°C) for Ni/graphite under vacuum (*6*), and

115° (1550°C) for Ni–C on graphite (*7*).

To obtain a more fundamental understanding of the mechanism of wetting and of the factors influencing the nickel interaction on graphite, a treatment of the interfa-

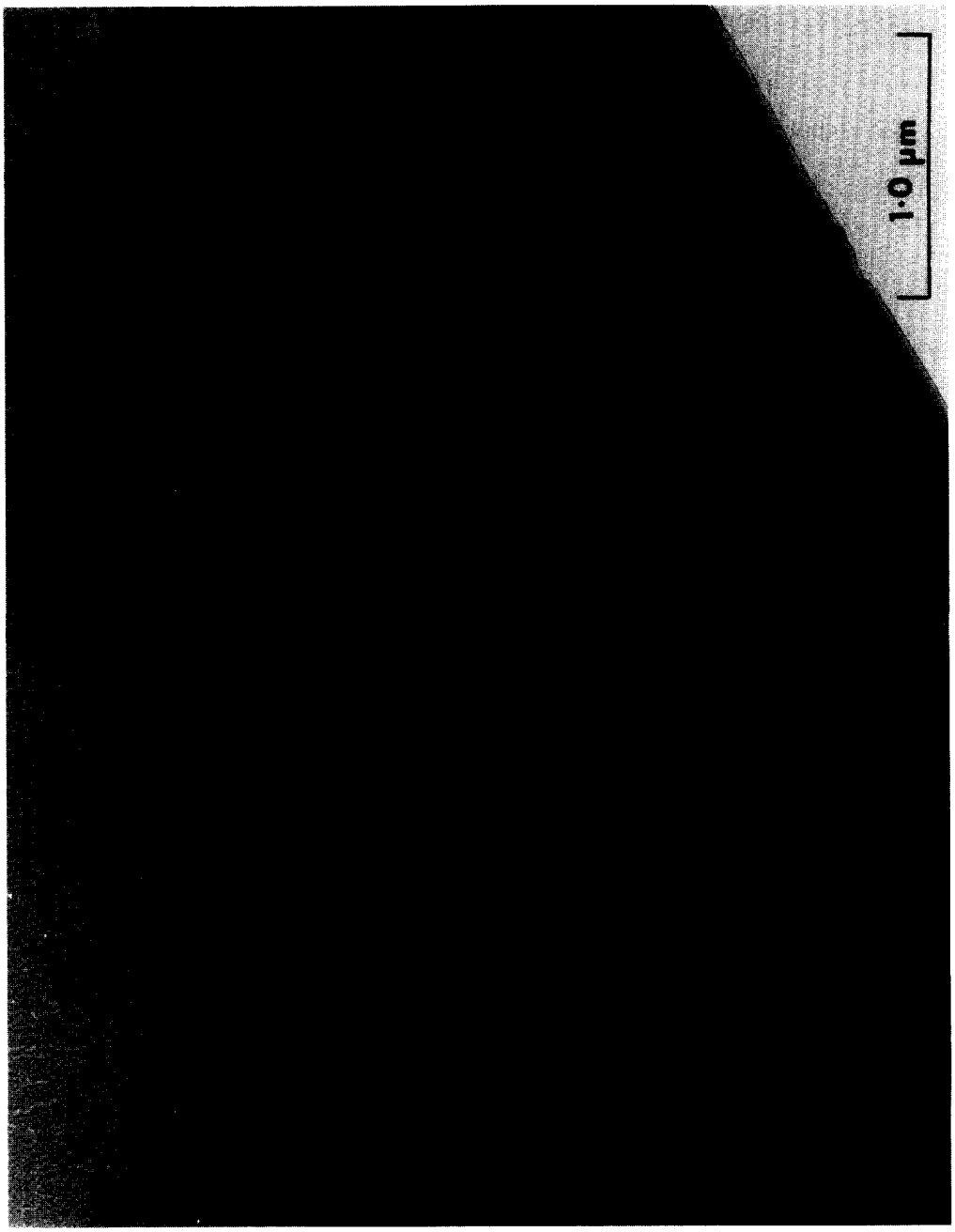

FIG. 1. Micrograph of a shadowed specimen of nickel/graphite which has been treated in 1.0 Torr H_2 at 1050°C. The arrows indicate the direction of the shadow across the surface.

cial forces affecting the wettability of metal melt–solid substrate is given below.

The contact angle Θ of the molten nickel particle on the graphite surface is related to the interfacial tension parameters by Young's equation:

$$\gamma_C = \gamma_{MC} + \gamma_M \cos \Theta, \qquad (1)$$

where γ_C (gas–support), γ_{MC} (metal–support), and γ_M (gas–metal) are the three interfacial tensions. Using the adopted value for $\gamma_M = 1860$ ergs $\cdot$ cm^{-2} (viscous or fluid nickel) (*8*) and $\gamma_C = 4600$ ergs $\cdot$ cm^{-2} (the value for the zigzag face or ⟨1120⟩ direction of graphite (*9*) one calculates (a) for the nickel particles that *wet* the graphite

$$\gamma_{MC}^{W} = 4118 \text{ ergs} \cdot \text{cm}^{-2}$$

and (b) for nickel particles that *do not wet* the graphite

$$\gamma_{MC}^{NW} = 5530 \text{ ergs} \cdot \text{cm}^{-2}.$$

This suggests that wetting is expected in H_2 when $\gamma_{MC} < \gamma_C$ and that the inactivity of some particles may be due to surface Ni–C formation.

(*B*) *Channeling action of nickel particles.* This interpretation can also be extended to account more quantitatively for many of the characteristics of the channels highlighted earlier (*2*), in particular the following aspects:

(a) channels emanate from *edges*,

(b) *small* particles are *first* to channel,

(c) *large* particles channel at *the fastest* rate at a given temperature,

(d) a particle that *meets* a channel has a tendency to be *reflected*, rather than cross the channel, and

(e) channels produced in H_2 are parallel to the ⟨1120⟩ crystallographic orientations. All these features were discussed in detail previously (*2*).

(*C*) *Redispersion of nickel along the channels.* Under the conditions where the redispersion phenomenon occurs (>1000°C) nickel is above its Tammann temperature (625°C), calculated at 0.52 bulk melting point (°K). The Tammann point is the temperature of onset of mobility of lattice atoms, and in a system where there are relatively weak interactive forces between particle and support one would expect to see particle motion at this temperature. We may therefore assume that some degree of atomic mobility exists within the nickel particles, i.e., they probably have a "soft core." If we also postulate that as the particles propagate channels they leave behind a film of nickel of uniform thickness on the walls (zigzag faces) of the channel, then when complete metal particle depletion has occurred:

N atoms in nickel particle = N dispersed atoms;

therefore,

$$\frac{V \cdot \delta \cdot N}{M} = 2 \sum_i (L_i D_i) \eta_{Ni}, \qquad (2)$$

where

V = volume of the nickel particle,
δ = specific gravity of nickel (8.902 g $\cdot$ cm^{-3}),
M = atomic weight of nickel (58.71),
N = Avogadro's number,
L_i = length of a channel in region i,
D_i = depth of a channel in region i,
η_{Ni} = number of nickel atoms per unit surface area.

In order to calculate the volume of the nickel particle the shape of the initial particle (in the early stages of its activity) is best approximated by a cylinder of diameter W and height D covered by a hemisphere of diameter W, as depicted in Fig. 2. This shape was chosen because it takes into account the observed contact angles between the particle and the graphite and is compatible with a periodic decrease in the channel width as observed in region C and discussed later. Other shapes could also satisfy these requirements, but this is not a critical issue since it is only being used to demonstrate that the redispersion phenomenon is due to the wetting and spreading effect.

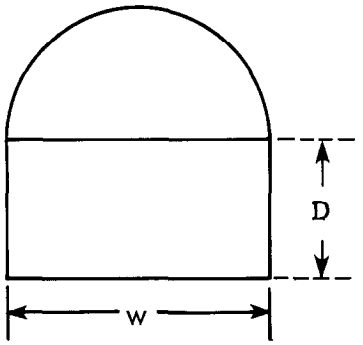

FIG. 2. Proposed initial shape of nickel catalyst particle.

Using the assumed particle shape, the volume is given by

$$V = \frac{\pi}{4} \cdot W^2\left(D + \frac{W}{3}\right); \qquad (3)$$

as $D/W = 0.25$ (from shadowing experiments) one gets as a rough approximation

$$V = \frac{7\pi W^3}{48}.$$

This model predicts that the width and depth of the channel may stay constant until 57% of the particle has been dispersed, i.e., until complete depletion of the hemispherical cap.

Let us now consider the spreading action of nickel in a typical linear channel for which $W = 37.5$ nm and $L = 2050$ nm. According to Eq. (2) we can write

$$\frac{7}{48}\pi(37.5)^3 \times \frac{8.902}{58.71} \times 10^{-21} \times 6 \times 10^{23} = 2 \times 2050 \times (37.5 \times 0.25) \times \eta_{Ni} \qquad (4)$$

leading to $\eta_{Ni} = 57$ atoms/nm^2 (if nickel depletion occurs only on sidewalls of the channel).

If one also considers depletion on the basal plane, then the right-hand side of Eq. (4) becomes equal to $(2LD + LW)\eta_{Ni}$, leading to $\eta_{Ni} = 19$ atoms/nm^2.

The actual value of η_{Ni} will probably be somewhere between these extremes, $19 < \eta_{Ni} < 57$, as some nickel will undoubtedly be deposited on basal plane defects.

These values can be compared with some typical calculated values for η_{Ni}.

Two situations will be considered:

(a) Close packing of nickel atoms (hexagonal parking)

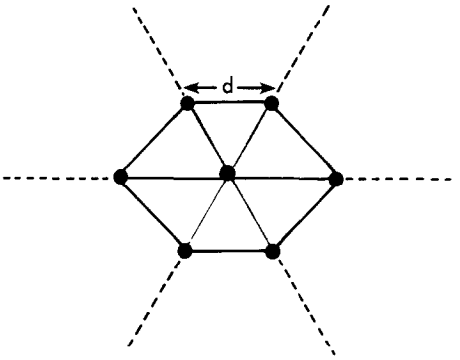

The number of nickel atoms per "surface" unit cell is 3, the corresponding area being $3(3)^{1/2}d^2/2 = 0.161$ nm^2. Hence, $\eta_{Ni} = 18.63$ atoms/nm^2.

(b) Regular packing of nickel atoms matching the graphite zigzag sublattice

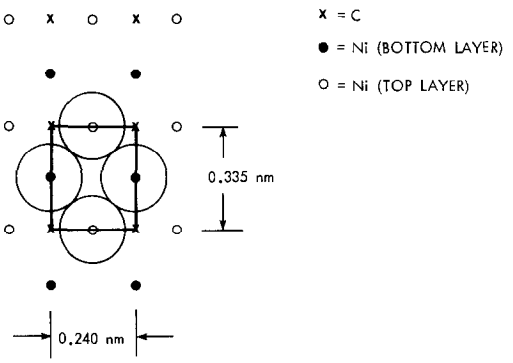

In this configuration, two atoms will be accommodated per "surface" unit cell, leading to $\eta_{Ni} = 24.8$ atoms/nm^2. These model values for the nickel packing density indicate that the nickel layer which is deposited on the channels will be nearly "monomolecular."

Figure 3 is a sequence showing the gradual loss of activity of a nickel catalyst particle and in Fig. 4 the three regions where the particle appears to exhibit diverse behaviors are highlighted. From the CAEM study, we were able to observe directly the detailed change in particle shape (top view,

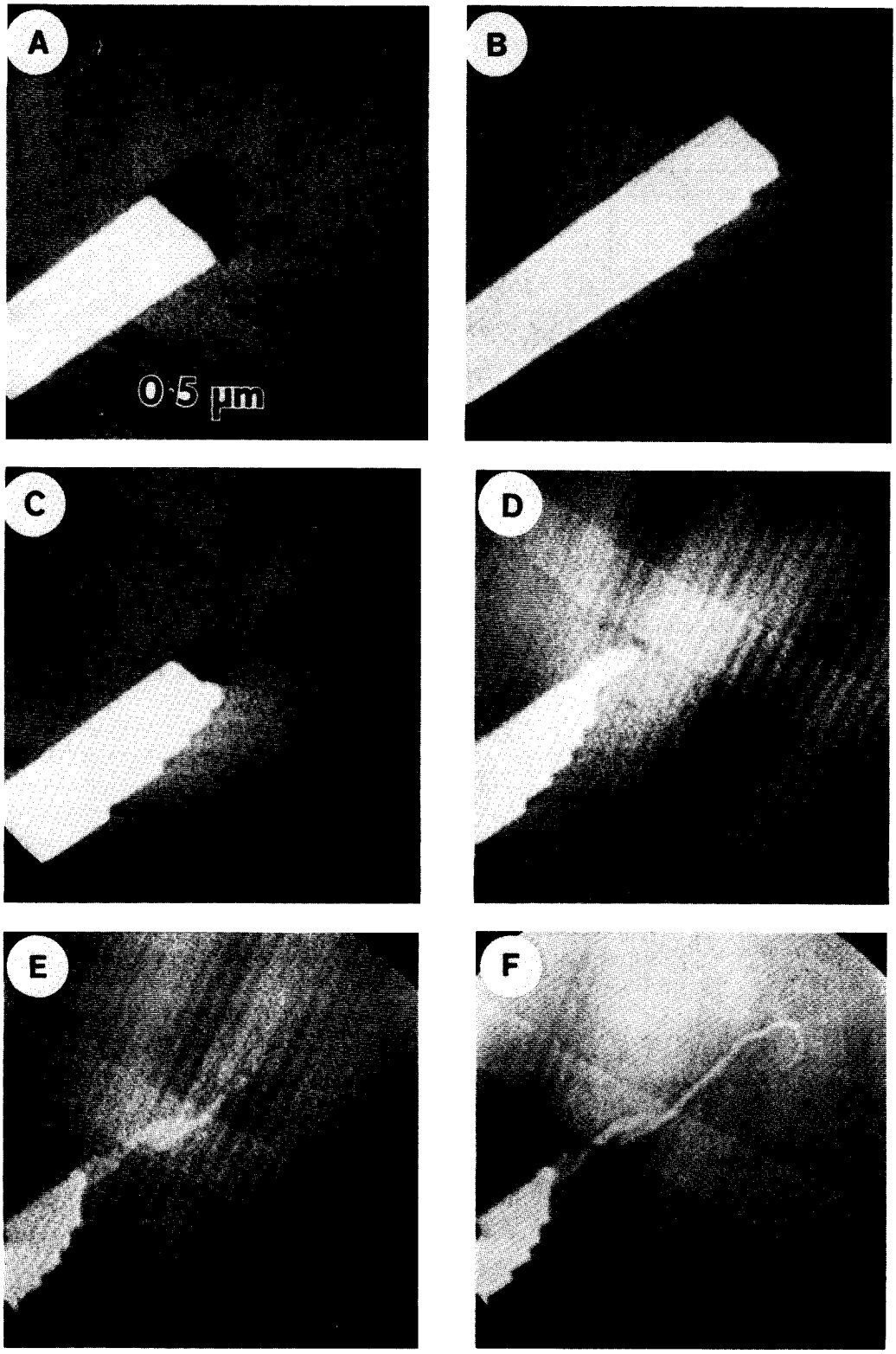

FIG. 3. Sequence showing the gradual loss of activity of nickel catalyst particle caused by deposition of metal along the edges of the channel.

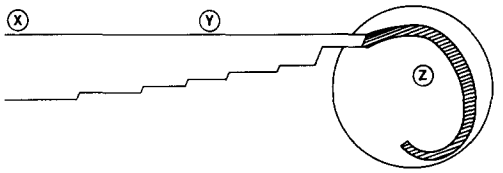

FIG. 4. Schematic representation of the channel shown in Fig. 3, highlighting the three regions of diverse particle behavior.

Fig. 5). Some corresponding shapes compatible with the observed narrowing of the channels for the "end on" and "side view" of the particle are also given in Fig. 5. As the particle traverses region X, we suggest that there is a progressive depletion in the size of the particle, but the width and depth remain constant until the "limiting situation" is reached. At this point about 60% of the nickel is lost, although the width of the particle has only decreased by about 25% (volume α radius^3). As the particle moves into region Y, surface tension forces begin to play an important role in the reaction. This is also the region where most of the changes occur, since the surface-to-volume ratio of the particle increases rapidly and as a consequence the temperature of the particle will also increase, eventually leading to a completely molten entity in region Z. The governing factors controlling particle behavior are summarized in Table 2.

A typical channel termination sequence (region Y) is quantitatively analyzed in Fig. 6. It is seen that the particle volume decreases sharply as it moves forward because of the spreading of nickel. The original channel depth, constant to the tip (where the whole particle ultimately melts), as seen from the shadowing experiments is 62.5 nm, i.e., 0.25 × 250 nm.

Figure 7 is a schematic representation of the change in volume of a particle accompanying the channel propagation process. The volume of the particle at stage (a) is $V = (\pi/4)D^2W$ (i.e., the volume at the start of region Y). For the limiting case, stage (b), the volume is

$$V_L = \frac{D^2W}{2}$$

so that $(V - V_L)/V = 0.36$, indicating that

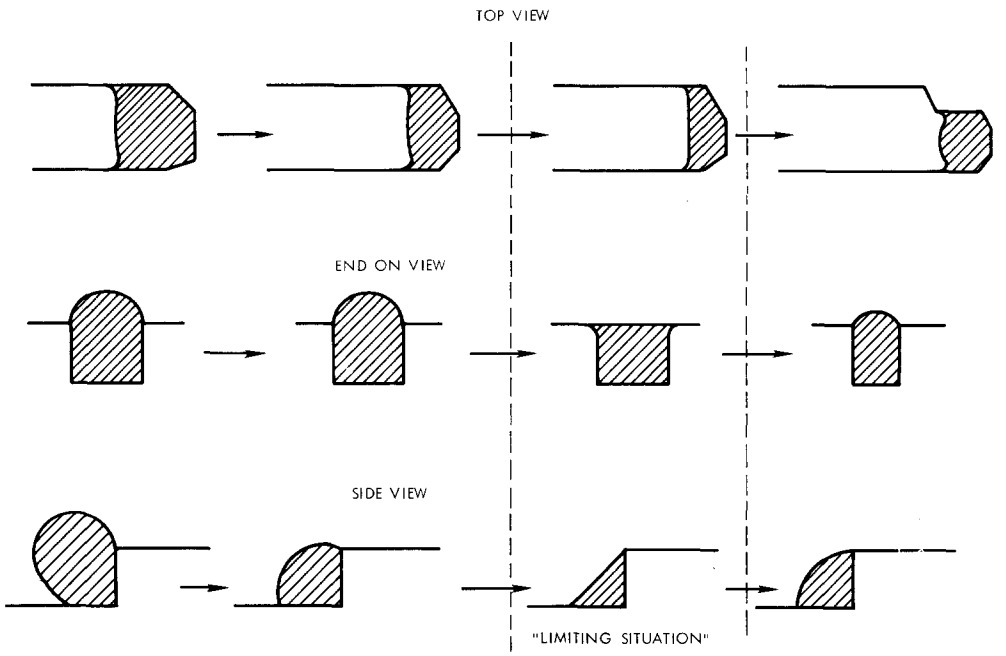

FIG. 5. Changes in the shape of the particle as it progresses from region X to region Y (Fig. 4).

TABLE 2

Controlling Factors in the Three Regions of Channel Formation

	Region A	Region B	Region C
System	Thin surface fluid layer and soft core	Thick surface fluid layer and soft core	Fluid particle (no core)
Governing factors	Soft core and preferred direction of motion	Soft core and surface tension forces	Erratic

the particle can theoretically lose at maximum 36% of its volume before it reorganizes under the influence of surface tension forces. Nickel which is lost from the particle is probably deposited on the channel walls.

The periodicity in the termination of the channels may be seen by computing the surface area of each region (a → f) (Table 3). Shrinkage occurs when the particle has lost 0.2–0.3 of its initial material in fair agreement with the proposed model.

Hydrogen Chemisorption Studies

Hydrogen chemisorption isotherms at room temperature, following various treatments, are described in Table 1 and shown in Figs. 8 to 11. It is clearly evident that the high-temperature-treated (≥1000°C) samples exhibit hydrogen uptakes which are rather unusual in shape and show a break near 100 Torr.

The hydrogen adsorption capacity of these samples is then best compared by considering uptake values at a given equilibrium pressure which we will select arbitrarily to be 200 Torr. Data are compiled in Table 4. It is seen that:

(i) After treatment in H_2 at 1095°C, both the first and second (following evacuation at room temperature) hydrogen uptakes give identical results and hence do not exhibit any "irreversible" hydrogen adsorption.

(ii) Evacuation at 1000°C suppresses the hydrogen adsorption ability.

(iii) The latter property can be restored by steaming at 1000°C.

It was also observed that following H_2 treatment at 1000°C and evacuation at

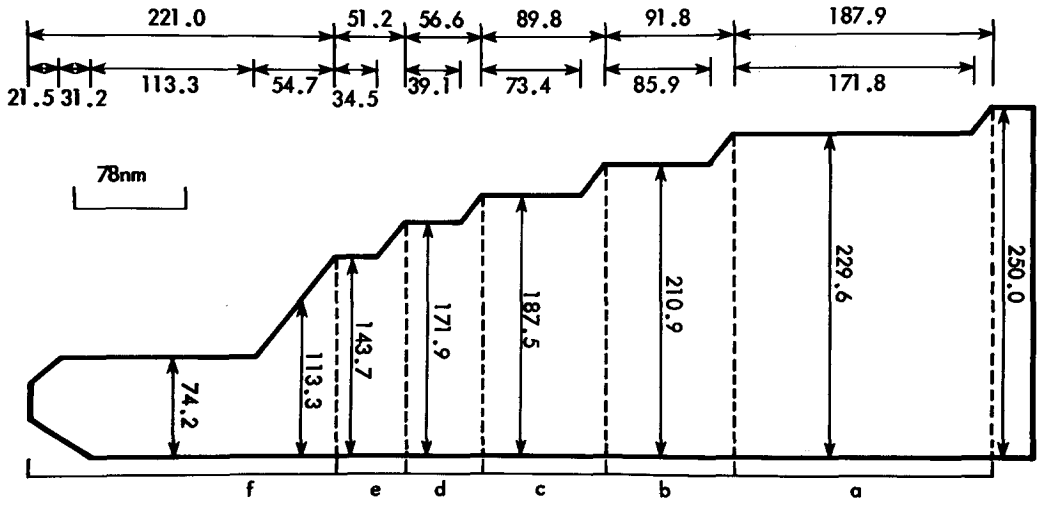

FIG. 6. Quantitative analysis of the channel termination region Y (Fig. 4).

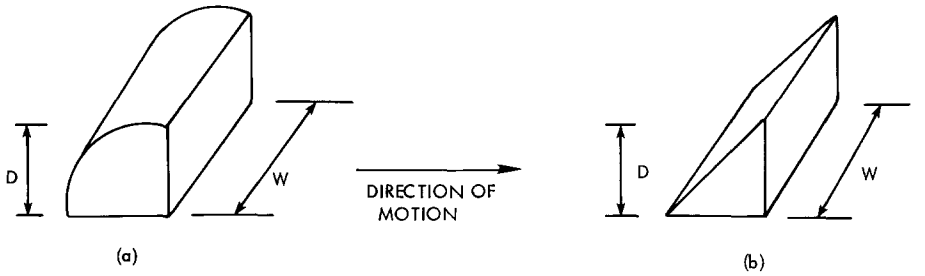

FIG. 7. Change in volume of particle accompanying reaction.

550°C, heating of nickel/Grafoil samples at 1000°C in a closed manifold led to a noticeable increase in pressure. The estimated amount of gas released under these conditions (D_1) is ~0.6 cm^3 STP · g^{-1} of catalyst.

This observation is paralleled by the electron microscopy data which showed that graphite gasification still occurred at 725°C for a certain time when hydrogen was replaced by an inert gas (*2*). This is a clear indication that graphite may act as a reservoir for (atomic) hydrogen which, when released, will gasify graphite to methane.

The absence of strong H_2 chemisorption following the high-temperature treatment in hydrogen, as well as the decrease in reversible hydrogen uptake, can be accounted for in terms of a chemical and/or electronic modification of nickel caused by its interaction with either carbon or sorbed hydrogen.

In the proposed model, discussed in detail in Ref. (*10*), nickel is progressively laid

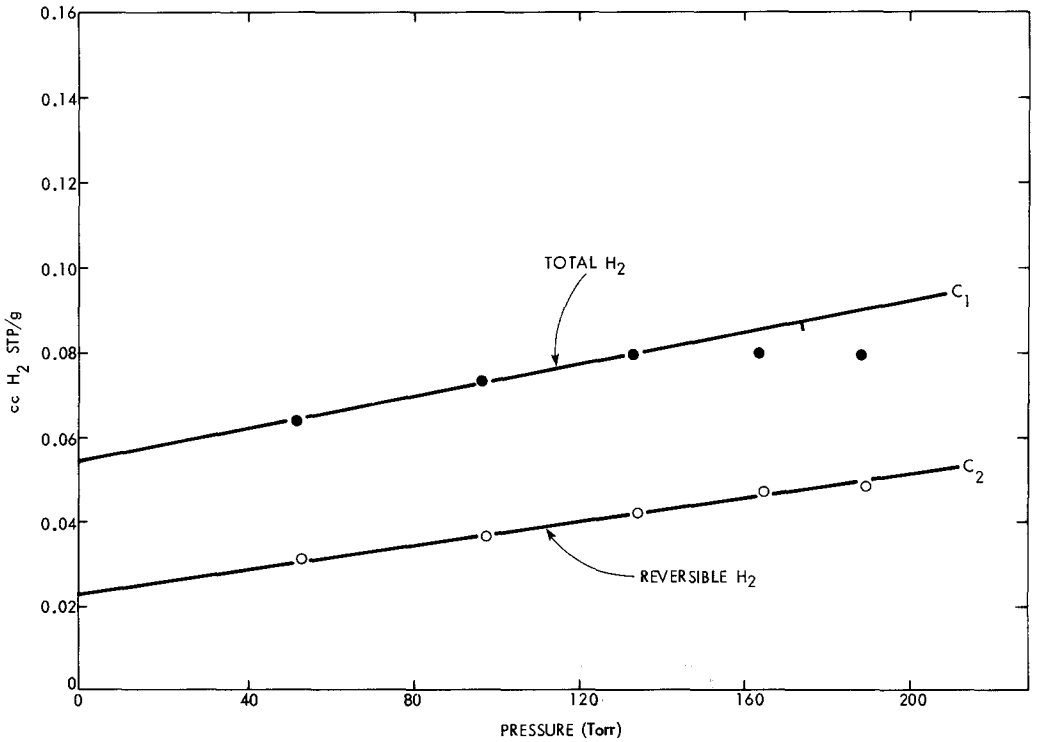

FIG. 8. Hydrogen adsorption isotherms at room temperature on a 2.66% nickel/Grafoil catalyst. Total, initial H_2 isotherm after reducing the sample at 600°C for 2 hr. Reversible, H_2 isotherm after evacuating sample following the initial isotherm for 15 min at room temperature.

TABLE 3

Computation of the Areas of Each Region (a → f) of the Channel during the Termination Sequence Shown in Fig. 6

Region	Area of basal plane surface (nm^2)	Area of lateral plane surfaces (nm^2)	Total surface area (nm^2)	R^a
a	4.31×10^4	2.35×10^4	6.66×10^4	0.331
b	1.94×10^4	1.15×10^4	3.09×10^4	0.23
c	1.68×10^4	1.12×10^4	2.80×10^4	0.27
d	9.72×10^3	7.07×10^3	1.68×10^4	0.22
e	7.36×10^3	6.40×10^3	1.38×10^4	0.23
f	1.74×10^4	2.76×10^4	4.5×10^4	—

[a] R = a/(a + b + . . . + f), or b/(b + c + . . . + f), or c/(c + . . . + f), etc.

TABLE 4

Chemisorption of Hydrogen on Nickel/Grafoil Catalysts

Run		Treatment[a]	Volume H_2 adsorbed[b]
1	C_1	Reduced 600°C, total	0.090
	C_2	Reduced 600°C, reversible	0.048
	C_3	Treated 1095°C in H_2, 2 hr	0.020
	C_4	Evacuated 25°C, following C_3	0.023
	C_5	Evacuated 1000°C	0.0
	C_6	Steaming 800°C	0.0
	C_7	Steaming 1000°C	0.042
2	C_3'	Reduced 600°C, treated 1000°C in H_2, 1 hr	0.0
	C_6'	Steamed 1000°C, 1 hr	0.042
	C_8'	Reduced 600°C	0.052

[a] See Table 1 for details.

[b] Value at an equilibrium pressure of 200 Torr and 25°C (cm^3 H_2 STP/g of catalyst).

down primarily on the walls and at defects on the basal plane of the channels while the particles move forward. Nickel deposited in this manner will strongly interact with sorbed hydrogen and therefore should be poorly active for C–C bond breaking (gasification of graphite) and strong H_2 chemisorption.

In contrast, the absence of Ni–H interac-

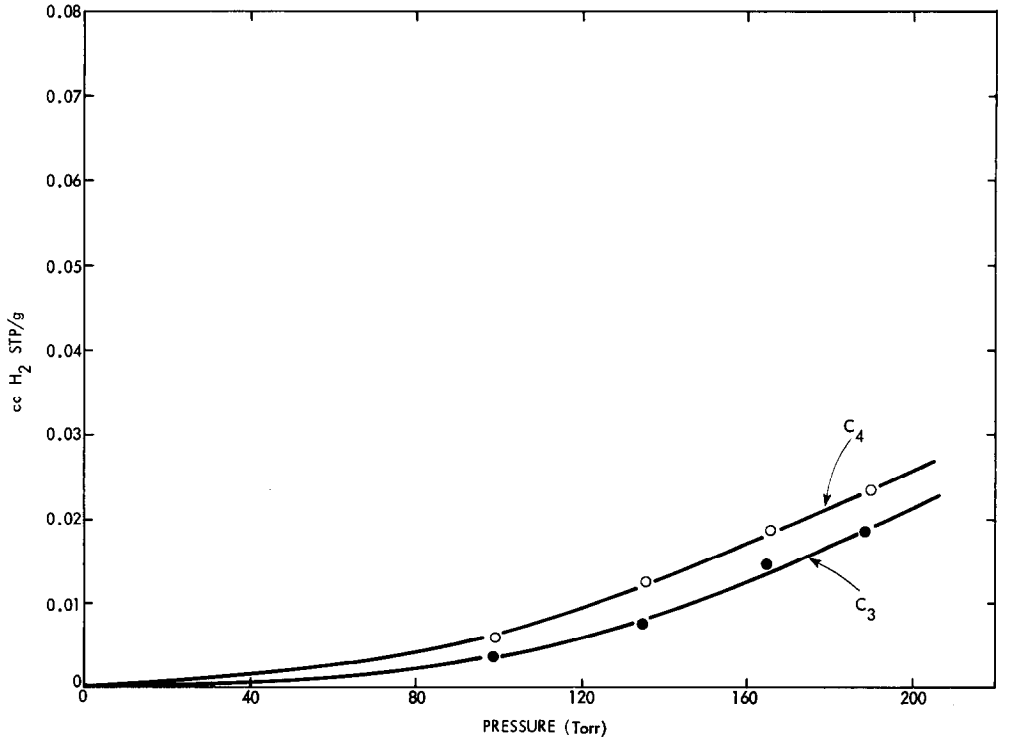

FIG. 9. Hydrogen adsorption isotherms at room temperature on a nickel/Grafoil catalyst. C_3, after reducing the sample at 1095°C for 2.0 hr; C_4, after evacuating the sample for 15 min at room temperature.

tions may result in the formation of Ni–C interactions (a surface Ni carbide which does not adsorb H_2). This will occur mainly upon evacuation at high temperatures and may thus account for the lack of hydrogen chemisorption in runs C_5 and C_6. It is also seen that steaming at 800°C is not sufficient to restore the hydrogen adsorption capacity; temperatures for the latter should be higher than 1000°C. Reasons for this may be that the Ni–C bonds are not effectively broken by H_2O at 800°C or that the sorbed H_2 is not released to a large extent below 1000°C.

The lack of chemisorption (C_6) may result from:

(i) sintering during the H_2 evacuation step at 1000°C (one could argue that since heating in H_2 leads to wetting and spreading of Ni particles on graphite, removal of H_2 should result in particle growth);

(ii) formation of a "surface carbide" in the absence of H_2.

The X-ray diffraction data obtained for nickel/Grafoil specimens after various treatments are given in Table 5, along with corresponding H_2 chemisorption information. They reject the effect of sintering and confirm that redispersion has indeed occurred at 1000°C (smaller particles being observed). Hence the formation of surface Ni–C on smaller (inactive) particles should be expected.

CONCLUSIONS

(1) The absence of strong hydrogen chemisorption following treatment in H_2 at 1000°C is due to H–Ni–C interactions which probably modify the electronic structure of highly dispersed Ni.

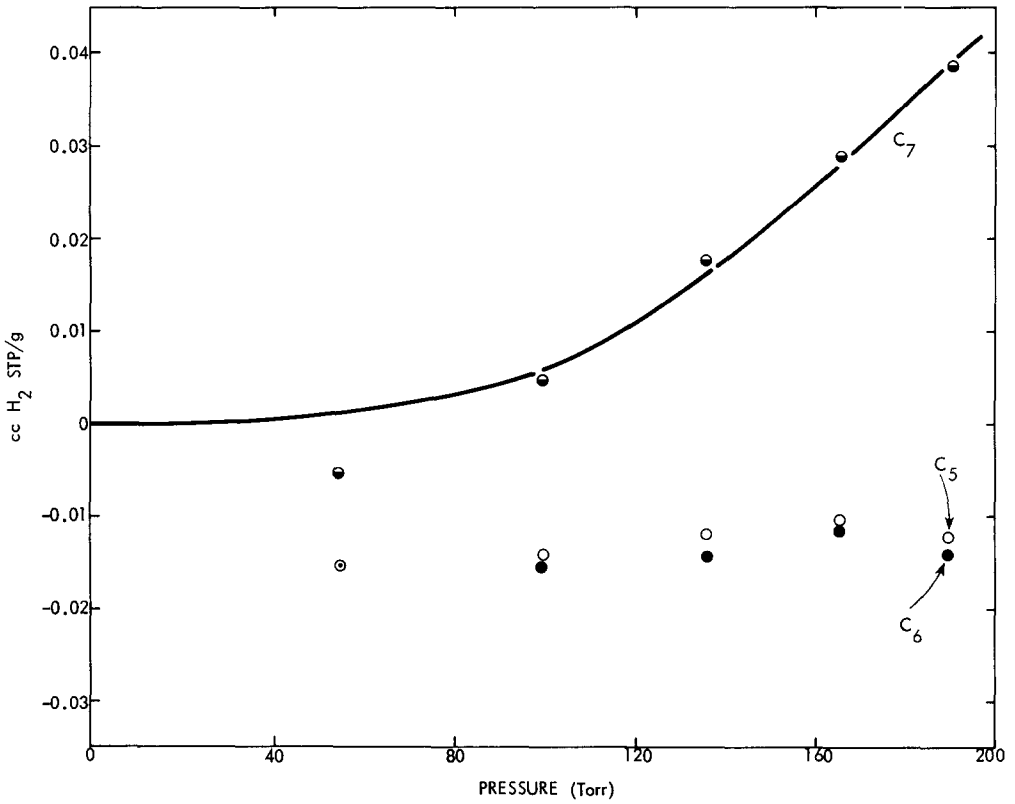

FIG. 10. Hydrogen adsorption isotherms at room temperature on a nickel/Grafoil catalyst. C_5, after evacuation at 1000°C for 10 min; C_6 after steaming at 800°C followed by evacuation at room temperature for 0.2 hr; C_7, after a further steaming at 1000°C and evacuation at room temperature.

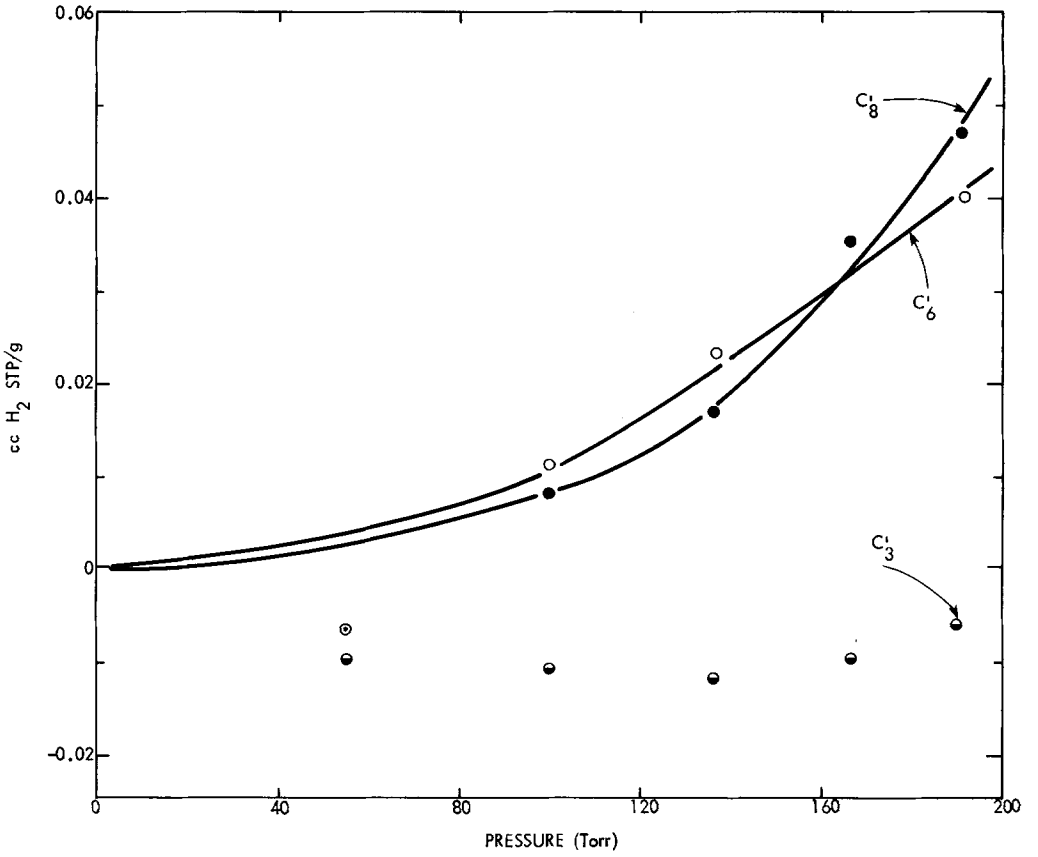

FIG. 11. Hydrogen adsorption isotherms at room temperature on a nickel/Grafoil catalyst. C'_3, after room treatment in H_2, at 1095°C for 1.0 hr, and evacuation at room temperature; C'_6, following steaming at 1000°C; and C'_8, after further treatment of the sample in H_2 at 600°C for 2.0 hr.

(2) The reversible hydrogen adsorption is diminished by high-temperature treatment: completely when H_2 is removed, less so if H_2 is present, because of the formation of a surface Ni–C-like compound.

(3) Ni–C bonds are broken up by steaming at 1000°C and the hydrogen chemisorption capacity is restored.

(4) Hydrogen may be sorbed in graphite, most probably in the atomic state, by heating nickel/Grafoil specimens at 1000°C in H_2.

TABLE 5

X-Ray Diffraction and Chemisorption Data on Treated Ni/Grafoil Specimens

Treatment	H_2 chemisorption and X ray
1. Reduced at 600°C	Large particles and normal H_2 chemisorption
2. Reduced at 600°C, treated in H_2 at 1000°C, evacuated at 950°C followed by steaming at 800°C	Smaller particles, but poor H_2 chemisorption, about zero (see C_6–Table 4)

The particle description used throughout this discussion is based on an extension of the hard-core model (*11*), but in the present system the particles do not possess a hard core as Ni is above its Tammann temperature (625°C). We believe that the surface layers of the particles will be hotter than the bulk because of heat released in the gasification reaction. Further, a high degree of

particle mobility on the graphite surface is expected as all atoms in the particles have some mobility at temperatures greater than 625°C.

ACKNOWLEDGMENTS

The authors would like to acknowledge the help of M. Estadt and J. Ziemiak in the samples preparation and the chemisorption measurements, respectively.

REFERENCES

1. Keep, C. W., Terry, S., and Wells, M., *J. Catal.* **66,** 451 (1980).
2. Baker, R. T. K., and Sherwood, R. D., *J. Catal.* **70,** 198 (1981).
3. Baker, R. T. K., and Harris, P. S., *J. Sci. Instrum.* **5,** 793 (1972).
4. Hennig, G. R., *in* "Chemistry and Physics of Carbon" (P. L. Walker, Jr., Ed.), Vol. 2, p. 1. Dekker, New York, 1966.
5. McVicker, G. B., Garten, R. L., and Baker, R. T. K., *J. Catal.* **54,** 129 (1978).
6. Weisweiler, W., and Mahadevan, V., *High Temp. High Pressures* **4,** 27 (1972).
7. Naidich, V. U., and Kolesnichenko, G. A., *Poroshk. Metall.* **6,** 55 (1961).
8. Tyson, W. R., and Miller, W. A., *Surf. Sci.* **62,** 267 (1977).
9. Abrahamson, J., *Carbon* **11,** 337 (1973).
10. Simoens, A. J., Derouane, E. G., and Baker, R. T. K., *J. Catal.* **75,** 175 (1982).
11. Derouane, E. G., Baker, R. T. K., Dumesic, J. A., and Sherwood, R. D., *J. Catal.* **69,** 101 (1981).